Journal of Inflammation Research

Dovepress
Taylor & Francis Group

Open Access Full Text Article

ORIGINAL RESEARCH

Comprehensive Analysis of Ferroptosis Markers in Lupus Nephritis Based on Bioinformatics Analysis and Experimental Validation

Su Zhang[1,2,*], Weitao Hu[3,*], Chunyan Huang[4], Xinxin Lin[4], Xiaoqing Chen[2]

[1]The Second Clinical College of Fujian Medical University, Quanzhou, People's Republic of China; [2]Department of Rheumatology, The Second Affiliated Hospital of Fujian Medical University, Quanzhou, People's Republic of China; [3]Department of Gastroenterology, The Second Affiliated Hospital of Fujian Medical University, Quanzhou, People's Republic of China; [4]Department of General Practice, The Second Affiliated Hospital of Fujian Medical University, Quanzhou, People's Republic of China

*These authors contributed equally to this work

Correspondence: Xiaoqing Chen, Email chenxiaoqing202203@163.com

Introduction: Lupus nephritis (LN) is a common and severe complication of systemic lupus erythematosus (SLE). Ferroptosis is a form of iron-dependent cell death induced by lipid peroxidation. However, its specific role in LN remains unclear.

Methods: We utilized the GSE32591 obtained from the GEO database to identify differentially expressed genes (DEGs) and conduct enrichment analysis. Differentially expressed ferroptosis-related genes of LN (LNDE-FRGs) were derived by taking the intersection of DEGs and ferroptosis-related genes (FRGs). Three machine learning algorithms were applied to screen candidate key LNDE-FRGs. The expression of the key LNDE-FRGs was validated using external validation cohorts and clinical samples. The diagnostic value of the key LNDE-FRGs was then assessed by receiver operating characteristic curve (ROC) analysis. In addition, we investigated the correlation between the key genes and glomerular filtration rate (GFR), urinary protein and serum creatinine (Scr) in LN patients via the Nephroseq V5 database. Subsequently, we performed immune infiltrating cell analysis of LN kidney tissue using Cibersort. Finally, we validated the expression of the key gene CYBB by clinical samples and in vivo experiments.

Results: A total of 377 DEGs and 20 LNDE-FRGs were identified. Machine learning algorithms selected four candidate key LNDE-FRGs (*CD44*, *CYBB*, *TCF4*, and *PARP12*). However, only *CYBB* exhibited consistent expression trends in both the training and validation cohorts ($P < 0.05$). Immune infiltration analysis revealed that the expression levels of monocytes and M0 macrophages were significantly higher in the LN group than in the normal control group. In addition, there was a correlation between key genes and GFR, urinary protein and Scr. Finally, the expression level of *CYBB* was verified in lupus mice.

Conclusion: *CYBB* may be a ferroptosis-related biomarker in LN. This may provide new ideas for the clinical treatment and pathogenesis of LN.

Keywords: lupus nephritis, ferroptosis, CYBB, immune infiltration, bioinformatics, machine learning

Introduction

Lupus nephritis (LN) is one of the most common and severe complications of systemic lupus erythematosus (SLE). Approximately 50% of SLE patients develop LN, and about 10% progress to end-stage renal disease, which impacts patients' daily lives and productivity, leading to anxiety, depression, and other psychological issues.[1,2] Currently, the treatment of LN primarily involves immunoregulation and immunosuppression. However, existing drugs such as glucocorticoids, cyclophosphamide, and mycophenolate mofetil have notable toxic side effects, including cardiovascular risks, osteoporosis, and infections.[3–5] Despite the emergence of new biologics such as belimumab, rituximab, and adalimumab offering hope for patients with refractory lupus, their high costs and uncertainty regarding long-term efficacy limit their widespread clinical application. Therefore, there is a need for better treatment strategies. So, exploring and refining the pathogenesis of LN and identifying new candidate targets for its treatment has become a hot topic in

Received: 11 March 2025
Accepted: 30 July 2025
Published: 12 August 2025

current research. Bioinformatics and machine learning (ML) techniques have shown promise in improving the precision of disease diagnosis and treatment by analyzing complex biological data and uncovering valuable genetic patterns.[6]

Ferroptosis is a novel form of cell death distinct from traditional programmed cell death, first proposed by Dixon et al in 2012. It is characterized by disturbances in iron metabolism, lipid peroxidation, and inhibition of the antioxidant system.[7,8] There is increasing evidence suggests that ferroptosis is involved in various systemic diseases, including neurological disorders, myocardial ischemia/reperfusion injury, intestinal diseases, and tumors.[9–12] Recent studies have shown that ferroptosis is associated with various kidney diseases, including acute kidney injury,[13] renal tumors,[14] and autosomal dominant polycystic kidney disease.[15] The main phenomena characterizing ferroptosis (lipid peroxidation, disturbances in iron metabolism, etc) can be observed in patients with SLE and positively correlate with disease activity in SLE.[16–21] Furthermore, major biochemical phenomena associated with ferroptosis, such as iron accumulation, significant reactive oxygen species (ROS) production, and glutathione peroxidase 4 (GPX4) depletion, have also been found in the kidneys of lupus nephritis mice models.[22–24] The use of ferroptosis inhibitors can reduce the infiltration of immune cells in the kidneys, decrease the production of autoantibodies and inflammatory cytokines, and improve proteinuria symptoms in LN mice.[22,25,26] Conversely, excessive infusion of iron-containing fluids or consumption of high-iron foods may trigger lupus.[27,28] Existing evidence suggests that ferroptosis is related to the occurrence and development of LN, and regulating ferroptosis may be a potential therapeutic target for LN. However, there is currently limited research on ferroptosis-related genes in LN, and the regulatory mechanisms of ferroptosis in LN remain unclear.

In this study, we utilized bioinformatics methods to gain gene expression matrix of LN patients' glomerular tissues from the GEO database. We performed differential expression analysis, functional enrichment analysis and constructed a protein-protein interaction network to get LNDE-FRGs. Three machine learning algorithms were employed in the study to identify candidate key LNDE-FRGs. The expression of the candidate key LNDE-FRGs was validated in two external datasets, and ultimately a key LNDE-FRG (*CYBB*) was identified. The diagnostic value of key LNDE-FRGs was evaluated by ROC analysis. The correlation between *CYBB* and clinical traits of LN was analyzed through the Nephroseq V5 database. Glomerular immune infiltration in LN and normal controls was quantified using the Cibersort algorithm based on gene expression profiling. In addition, the expression of *CYBB* was validated based on clinical renal tissue paraffin samples and animal models. The primary goal of these analyses is to provide new insights that could help in the prevention and treatment of LN.

Materials and Methods

Data Acquisition

Data from the GEO database (https://www.ncbi.nlm.nih.gov/geo/),[29] including the GSE32591,[30] GSE113342[31] and GSE200306[32] datasets, were downloaded. The GSE32591 is based on the GPL14663 platform and comprises 93 samples consisting of 32 LN glomerular tissues, 32 LN tubular tissues, 14 normal glomerular tissues, and 15 normal tubular tissues. A total of 46 glomerular samples were used in this study. The GSE113342 is based on the GPL21847 platform and contains 6 normal glomerular tissues, 14 LN first biopsies and 14 LN repeated biopsies of glomerular tissue. We selected 14 LN first biopsies and 6 normal glomerular tissues. The GSE200306 is based on the GPL21847 platform and includes 53 kidney tissue samples, of which 34 are LN kidney tissues and 19 are normal tissues. All kidney tissue samples were included in this study. Among them, GSE32591 was served as the training set and the other two as the validation set. We defined LN glomerular tissue as the LN group and normal glomerular tissue as the NC group. Details of the datasets included in this study are displayed in Table 1.

Table 1 Details of the Datasets Included in This Study

Dataset	Platform	Species	Tissue	Number of Cases and Controls	Type of Cohorts
GSE32591	GPL14663	*Homo sapiens*	Glomerular tissues	32 LN/14 NC	Training
GSE113342	GPL21847			14 LN/6 NC	Validating
GSE200306	GPL21847			34 LN/19 NC	Validating

Identification of DEGs

The microarray data of the GSE32591 was processed for residual value complementation, background correction and normalization with "limma" package.[33] DEGs were acquired through setting the screening conditions of adjusted $P < 0.05$ and |log2FC| > 0.585. The genes with adjusted $P < 0.05$ and $\log_2FC > 0.585$ were defined as significantly up-regulated genes, and the genes with adjusted $P < 0.05$ and $\log_2FC < -0.585$ were categorized as significantly down-regulated genes.

Enrichment Analysis of DEGs

Gene Ontology (GO) and Kyoto Encyclopedia of Genomes (KEGG) enrichment analysis were conducted on DEGs using the "clusterProfiler" package.[34] Significant biological processes (BP), cellular components (CC), molecular functions (MF), and signaling pathways associated with DEGs were identified. The $P < 0.05$ was deemed to be statistical significance.

Protein-Protein Interaction (PPI) Network Construction

The DEGs were uploaded to the STRING database (https://string-db.org/)[35] to construct a PPI network. Protein junctions were set to have a minimum interaction score of 0.4. Cytoscape (version 3.9.1)[36] was used to visualize the PPI networks. The molecular complex detection (MCODE) (version 2.0.3) plugin was applied to find the most important clusters.[37] The setup parameters for the MCODE plugin in this study are MCODE score > 5, Degree Criticality = 2, Node Score Criticality = 0.2, Maximum Depth = 100, k-score = 2.

Identification of LNDE-FRGs

The FRGs were gained from the ferroptosis-related database FerrDb V2 (http://www.zhounan.org/ferrdb/).[38] A total of 834 FRGs were downloaded for subsequent analysis. The overlapping genes of DEGs and FRGs were known as LNDE-FRGs. Meanwhile, a heatmap was used to display the distribution of LNDE-FRGs in the LN group and NC group.

Identification of Candidate Key LNDE-FRGs

The least absolute shrinkage and selection operator (LASSO) is a widely-used machine learning algorithm for fitting generalized linear models. It is well-known for its dual capability of variable selection and complexity regularization. LASSO regression employs the parameter λ to regulate the model's complexity.[39] When λ is increased, a greater penalty is applied to linear models with many variables, which reduces the number of selected genes. This results in a more streamlined and representative set of key genes in the outcomes. In this study, LASSO regression analysis of LNDE-FRGs was performed using the "glmnet" package for R.[40] Random Forest (RF) is a machine learning technique that is implemented using the "randomforest" package for R.[41] Characteristic importance scores for each gene were determined by random forest and the genes with the top 10 importance values were selected. Support vector machine-recursive feature elimination (SVM-RFE) is a machine learning method commonly-used to screen feature genes. The model is trained with samples, and each feature is ranked in terms of score, after which the optimal combination of features is selected using the recursive feature elimination algorithm in a step-by-step iterative manner.[42] The intersecting genes of the three machine learning algorithms were extracted as candidate ferroptosis genes through the "VennDiagram" package of R.

Validation of the Key LNDE-FRGs

To check the accuracy of the candidate key LNDE-FRGs screened by machine learning, box plots were used to show the distribution and expression of the candidate key LNDE-FRGs in the training and validation cohorts. ROC analysis of key genes using the "pROC" package.[43] The diagnostic value of key genes was also evaluated by area under the ROC curve (AUC).

Correlation Analysis of Key LNDE-FRGs with Clinical Traits of LN

The key LNDE-FRGs were uploaded to the NephroSeq V5 database (http://v5.nephroseq.org)[44] for analysis and validation. In addition, the correlation of the key genes with GFR, proteinuria and Scr levels in LN was analyzed.

Analysis of Immune Cell Infiltration

Cibersort (https://cibersortx.stanford.edu/)[45] was performed to compute scores for 22 immune infiltrating cell types in LN and healthy control glomerular samples, repeated 1000 times. In addition, Pearson correlation analysis was performed to determine the correlation between the key LNDE-FRGs and the immune infiltrating cells, and the significance level was set at $P < 0.05$ with a Pearson correlation coefficient (r) > 0.35, indicating that there is a correlation between them.

Renal Tissue Section Experiments

Collection of Renal Tissue Sections

In order to ensure that LN patients were suitable, the exclusion criteria for this study were having diabetes, hepatitis, cirrhosis, or IgA nephropathy. Thirty patients diagnosed with LN by renal biopsy in the Department of Rheumatology of the Second Affiliated Hospital of Fujian Medical University from January 2023 to January 2024 were recruited with the consent of the patients or guardians. In addition, paraffin sections from 5 cm adjacent to the cancerous tissues of kidney cancer patients were collected from the Department of Pathology of the Second Affiliated Hospital of Fujian Medical University as control samples (NC group).

Immunohistochemical (IHC) Staining

Paraffin sections were first deparaffinized and hydrated. Next, thermal repair of antigens was performed to expose potential antigenic sites. Subsequently, non-specific binding sites on the surface of the sections were closed using a sealing solution. The specific primary antibodies (CYBB, 1:1000, 19013-1-AP, Proteintech; ACSL4, 1:500, 22401-1-AP, Proteintech; GPX4, 1:500, 30388-1-AP, Proteintech) were then added to bind to the target antigen, followed by the secondary antibody with HRP labeling. Finally, the slices were re-stained with hematoxylin and sealed with neutral gum. The results were observed under a microscope and photographed to record the results.

Animal Experimentation

Animal Selection

Four-week-old female C57BL/6 and MRL/lpr mice were purchased from Fuzhou Wu Laboratory Animal Co. Female MRL/lpr mice were selected as the spontaneous lupus mouse model, and female C57BL/6 mouse of the same age were used as the normal control.

Sample Acquisition

The mice were sacrificed at 16th week. Kidney and blood samples were obtained from mice under anesthesia. The kidneys were immediately removed, the envelope was quickly removed, one kidney was cut longitudinally, 1/2 kidney was fixed with 4% paraformaldehyde and embedded with OCT, respectively, and the other kidney was separated from the renal cortex and placed in a tissue freezing tube, quick-frozen with liquid nitrogen and then stored in the refrigerator at −80°C for subsequent extraction of renal cortical RNA and protein. Meanwhile, spleen index and perirenal lymph node index were weighed and calculated for each mouse. The mice were executed by intravenous injection of amobarbital at the end of the experiment.

Detection of Urinary Protein and Anti-dsDNA Antibody

Urine protein concentration was determined according to the instructions of the Bradford Protein Concentration Assay Kit (Beyotime, China), and mouse 24h urine protein was calculated in conjunction with mouse 24h urine volume. Mouse anti-dsDNA ELISA kit (Fujifilm, Japan) was utilized to detect anti-dsDNA antibody levels.

Periodic acid-Schiff (PAS) Staining

The sections to be stained are deparaffinized with xylene for 5–10 min. Dehydrate in different concentrations of alcohol for 3–5 min and then rinse in distilled water for 3 min. Next, the sections were stained with 1% periodate in Schiff's

solution protected from light for 20 min and washed with distilled water. The nuclei were restained by adding hematoxylin staining solution for 5 min, dehydrated again in ethanol and placed in xylene for 5 min. The staining was observed under the microscope after sealing with neutral gel.

Immunofluorescence (IF) Staining

Paraffin sections of mice kidney were deparaffinized and hydrated in ethanol and washed three times in PBS solution after addition of hydrogen peroxide. Subsequently antigen repair was performed and washed again with PBS solution. C3 antibody (ab97462, Abcam) or IgG antibody (ab172730, Abcam) was added and incubated overnight at 4°C. PBS was washed again and secondary antibody was added and incubated for 30 min at 37°C. PBS was washed 3 times and dye was added and incubated at room temperature for 10 min. PBS was washed 3 times, PBS was removed and the sections were viewed under a microscope and anti-fluorescence quenching sealer was added.

The Detection of Malondialdehyde (MDA), ROS and Glutathione (GSH)

As mentioned earlier, lipid peroxidation generating excess ROS as well as consuming more glutathione (GSH) is an important biochemical feature of ferroptosis. MDA (S0131S, Bryotime, Shanghai, China), GSH (A006-2-1, Jiancheng Bioengineering Institute, Nanjing, China) and ROS (S0033S, Bryotime, Shanghai, China) test kits were detected MDA, GSH and ROS levels in tissues. Operating according to the manufacturer's instructions.

Real-Time Quantitative Reverse Transcription Polymerase Chain Reaction (RT-qPCR)

The RNA extraction kit (R0027) was purchased from Bryotime (Shanghai, China). Reverse transcription reagents were purchased from Takara (Japan). Follow the appropriate instructions to extract cDNA. Finally, ABI PRISM 7500 PCR instrument (AppliedBiosystems, United States of America) was used to amplify the target gene. The primers for the genes involved in this study are shown in Table 2.

Western Blotting

Western blotting was used to detect the expression of β-actin (1:10000, 20536-1-AP, Proteintech, China), CYBB (1:5000, 19013-1-AP, Proteintech, China), ACSL4 (1:10000, 22401-1-AP, Proteintech, China) and GPX4 (1:1000, 30388-1-AP, Proteintech, China) in mouse kidney. Briefly, equal amounts of renal cortical fragments and protein samples were separated by sodium dodecyl sulfate-polyacrylamide gel electrophoresis (SDS-PAGE). After being closed with 5% skimmed milk powder for 2 h, the membrane was incubated with the corresponding primary antibody overnight at 4°C in a refrigerator. After washing the next day, the membranes were incubated with HRP-containing IgG (H+L) (1:10,000, SA00001-2, Proteintech, China) for 1 h at room temperature. Finally, positive bands were developed using the BeyoECL Plus color development kit and analyzed using an ImageQuant LAS4000mini imager.

Ethics Statement

The study was approved by the Ethics Committee of the Second Affiliated Hospital of Fujian Medical University under the ethical approval number [2024 (082)] and followed the Declaration of Helsinki. The patient and their family signed the consent form. The animal study protocol was approved by the Institutional Animal Care and Use Committee of Fujian Medical University and followed the standards of the National Institutes of Health Guide for the Care and Use of Laboratory Animals (SYSU-IACUC-2022-001210).

Table 2 The Primers for the Genes Involved in This Study

Gene symbol	Forward Primer	Reverse Primer
B-actin	CATTGCTGACAGGATGCAGAAGG	TGCTGGAAGGTGGACAGTGAGG
CYBB	TGTGGTTGGGGCTGAATGTC	CTGAGAAAGGAGAGCAGATTTCG
GPX4	CCTCTGCTGCAAGAGCCTCCC	CTTATCCAGGCAGACCATGTGC
ACSL4	CCTTTGGCTCATGTGCTGGAAC	GCCATAAGTGTGGGTTTCAGTAC

Statistical Analysis

All analyses were conducted using R software (version 4.3.3) and GraphPad Prism (version 10.1.2). The Student's *t*-test was used to compare differences in gene expression between the different groups. Pearson analysis was utilized to explore the correlation between core genes and immune infiltrating cells, and $P < 0.05$ was deemed statistically significant. A flowchart of the study is presented in Figure 1. Supplementary Table 1 displays the abbreviations of this study.

Results

Preprocessing for the Training Set

The median gene expression of individual samples in the training set GSE32591 was mixed before treatment and remained consistent after treatment, suggesting that potential batch effects were greatly mitigated, thus facilitating subsequent studies (Supplementary Figure 1).

Identification and Enrichment Analysis of DEGs

A total of 377 DEGs were screened, including 257 up-regulated and 120 down-regulated genes (Figure 2A and B). DEGs were detailed in Supplementary Table 2. GO enrichment of DEGs displayed that DEGs were mainly participated in biological processes (BP) such as type I interferon signaling pathway, neutrophil activation involved in immune response, positive regulation of cytokine production, and so on. In terms of cellular component (CC), DEGs were mainly enriched in collagen-containing extracellular matrix, vesicle lumen, membrane raft. DEGs mainly play a role in molecular functions (MF) such as extracellular matrix structural constituent, cytokine binding, and immune receptor activity

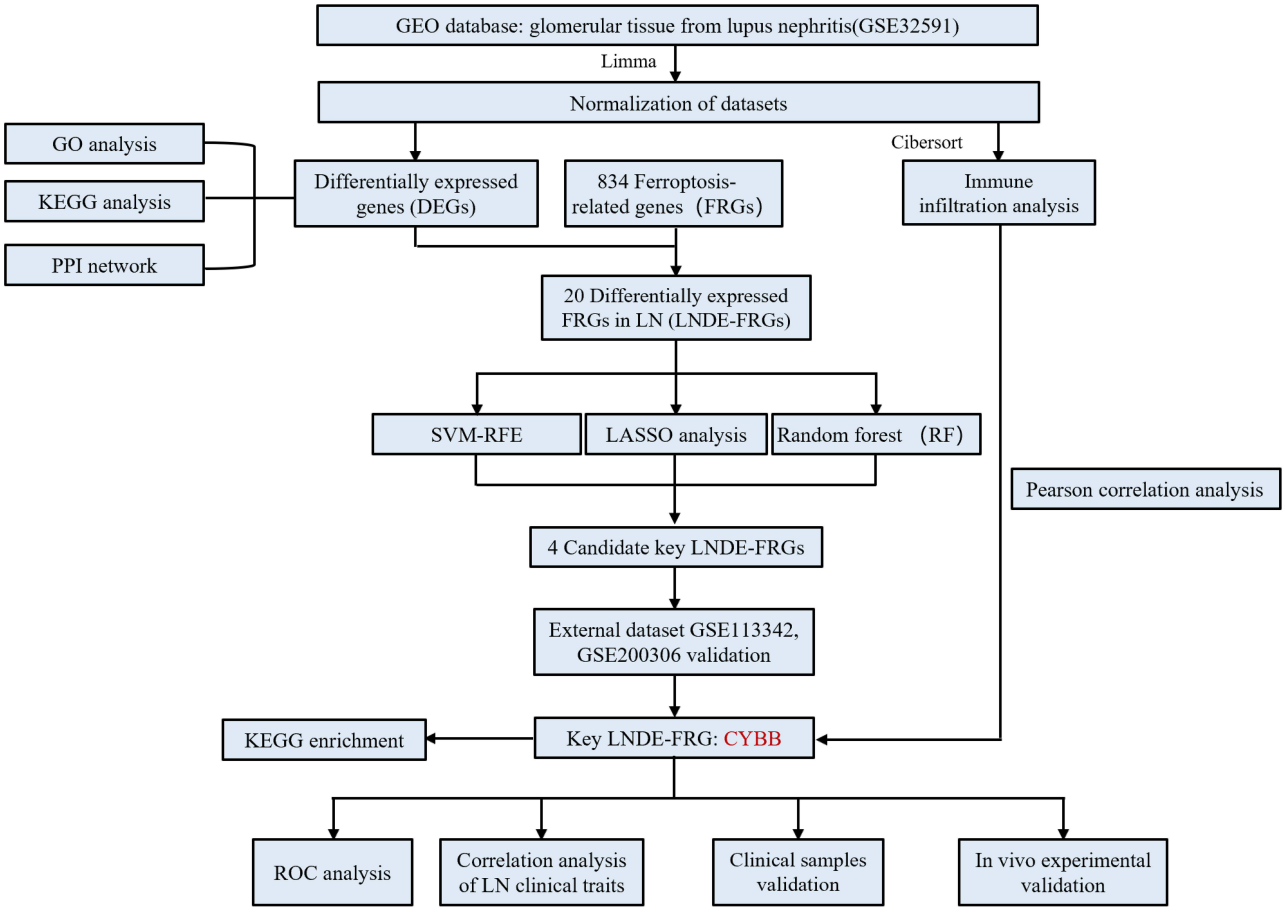

Figure 1 Flowchart of this study. The red font "CYBB" is the key ferroptosis-related gene in lupus nephritis in this study.

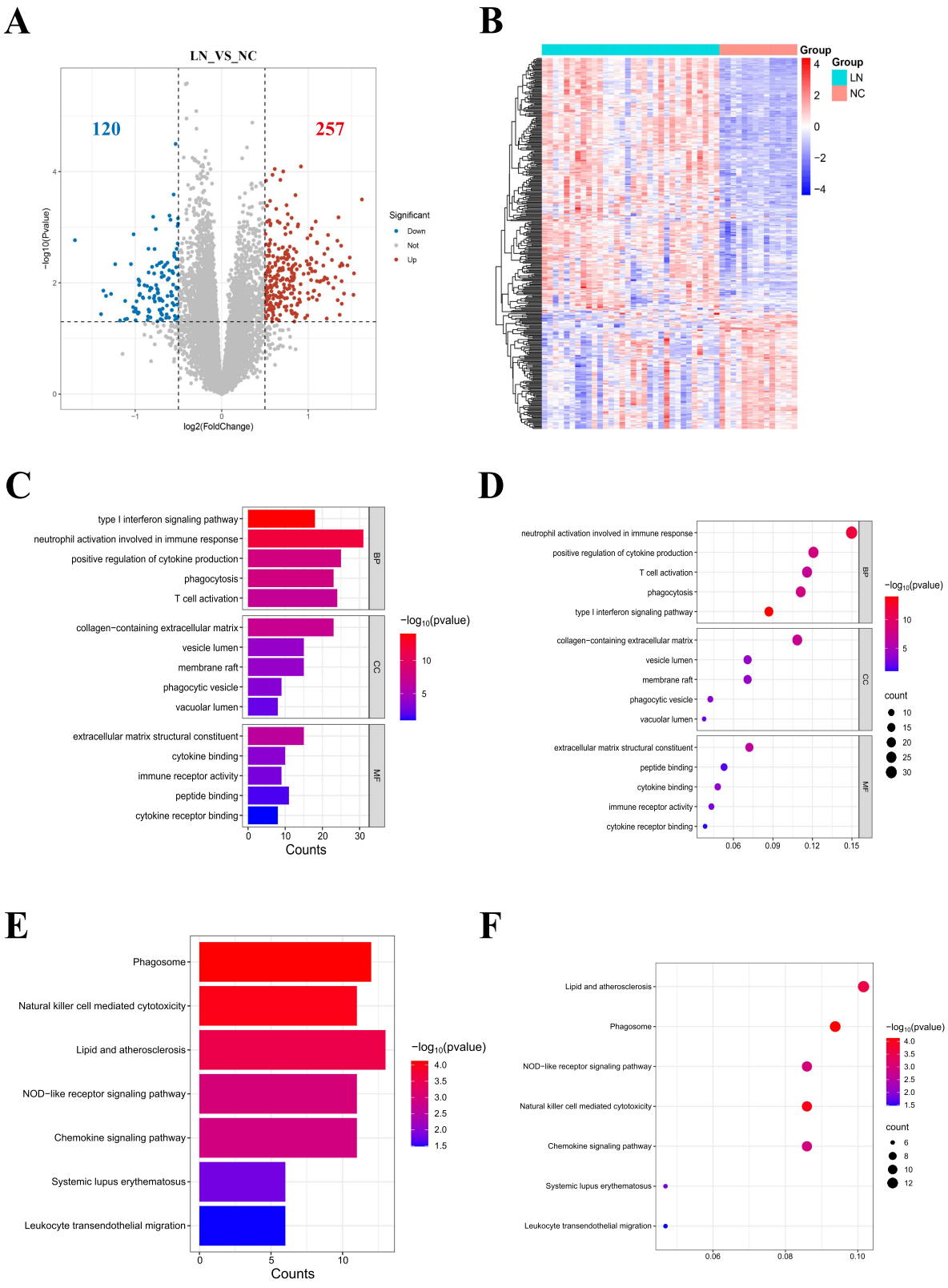

Figure 2 Identification of DEGs in LN and enrichment analysis. (**A**) The volcano plot displayed the DEGs. Red represents upregulated genes, while blue represents downregulated genes. (**B**) The heatmap showed the distribution of DEGs in LN and NC groups. (**C**) Bar plot of GO enrichment analysis. (**D**) Bubble plot of GO enrichment analysis. (**E**) Bar plot of KEGG enrichment analysis. (**F**) Bubble plot of KEGG enrichment analysis.

https://doi.org/10.2147/JIR.S527545

(Figure 2C and D). KEGG enrichment revealed that DEGs may be engaged in phagosome, natural killer cell mediated cytotoxicity, lipid and atherosclerosis, NOD-like receptor signaling pathway, chemokine signaling pathway, systemic lupus erythematosus (SLE) and leukocyte transendothelial migration (Figure 2E and F). The phagosome signaling pathway with the most significant enrichment was selected for display (Supplementary Figure 2).

Protein Interaction Network Connections and Identification of LNDE-FRGs

The PPI network constructed by uploading 377 DEGs to the STRING database was visualized using Cytoscape software. After removing isolated points, we got a PPI network consisting of 342 nodes and 2737 edges (Supplementary Figure 3A). The key module network acquired through the MCODE plug-in was an interactive network of 31 nodes and 284 edges (Supplementary Figure 3B), suggesting that these DEGs are closely related and their products are engaged in the same biological process. Then venn plot was derived for 20 LNDE-FRGs (Figure 3A). The heatmap displayed that there was a significant difference in the expression of the 20 LNDE-FRGs in the LN group and NC group (Figure 3B).

Identification of Candidate Key LNDE-FRGs

Three machine learning methods were implemented to select candidate key LNDE-FRGs from 20 LNDE-FRGs. The LASSO regression screened six genes, *CD44*, *CYBB*, *MICU1*, *PARP12*, *PLTP*, and *TCF4* (Figure 3C and D). The top 10 genes ranked by Random Forest in terms of importance for LNDE-FRGs were *PARP12*, *TCF4*, *CD44*, *BID*, *EZH2*, *CYBB*, *IR7*, *GCH1*, *TIGAR*, and *RRM2* (Figure 3E). While the SVM-RFE algorithm yielded a total of 13 genes (Figure 3F). Their crossover genes (*CD44*, *CYBB*, *TCF4* and *PARP12*) are the candidate key LNDE-FRGs (Figure 3G). The key genes generated by each algorithm are listed in Table 3. In addition, Supplementary Table 3 demonstrates the functions of the candidate key genes.

Identification and Evaluation of Key LNDE-FRGs

In order to test the accuracy of the candidate key LNDE-FRGs screened by machine learning, box plots were used to show the distribution and expression of the candidate key genes in the training and validation sets. We found that among the four candidate key genes, only *CYBB* showed the same expression trend in the training and validation sets with $P < 0.05$, so we finally identified *CYBB* as a key LNDE-FRG (Figure 3H–J). Interestingly, we observed that *CYBB* expression was elevated in all three LN-related datasets. ROC analysis was employed to evaluate the diagnostic value of *CYBB* for LN. The results showed that the AUC of *CYBB* in GSE32591 = 0.946. In GSE113342, the AUC = 1. While in GSE200306, the AUC = 0.688 (Figure 3K). In summary, *CYBB* offered a good value in predicting LN.

Immune Infiltration Cell Analysis

LN, as a typical autoimmune disease, inflammation and immune response play an essential role in its pathophysiologic process. In this study, immune cell infiltration in LN was analyzed through the CIBERSORT website. As shown in Figure 4A and B, we observed that these glomerular tissue samples had the highest levels and relative proportions of monocytes, followed by macrophages. And the level of monocyte infiltration was found to be significantly higher in LN than in NC. Then we further analyzed the correlation between immune cells in glomerular tissues of LN (Figure 5A). The differences in immune cell infiltration in LN and NC were also further compared by box plots. Analysis of differences revealed significant differences in immune cell infiltration in glomerular tissue between LN and NC groups (Figure 5B). Specifically, monocytes ($P < 0.001$), activated NK cells ($P < 0.01$), and M0 macrophages ($P < 0.01$) were significantly increased in LN patients; whereas in NC, naive B cells ($P < 0.01$), memory B cells ($P < 0.05$), resting CD4+ memory T cells ($P < 0.01$), follicular helper T cells ($P < 0.0001$), regulatory T cells ($P < 0.001$), resting NK cells ($P < 0.0001$), resting dendritic cells ($P < 0.001$), and neutrophils ($P < 0.01$) were significantly increased. These results suggested that myeloid cells, including monocytes and M0 macrophages, are the major infiltrating immune cells in the glomeruli of lupus nephritis. These cells may play an important function in the pathogenesis of LN.[46–48]

Finally, analysis of glomerular immune cell infiltration revealed an association between the CYBB and specific immune cells. Pearson correlation analysis showed that CYBB became positively correlated with M0 macrophages ($P < 0.01$) and monocytes ($P < 0.05$) and negatively correlated with resting CD4+ memory T cells ($P < 0.001$), resting

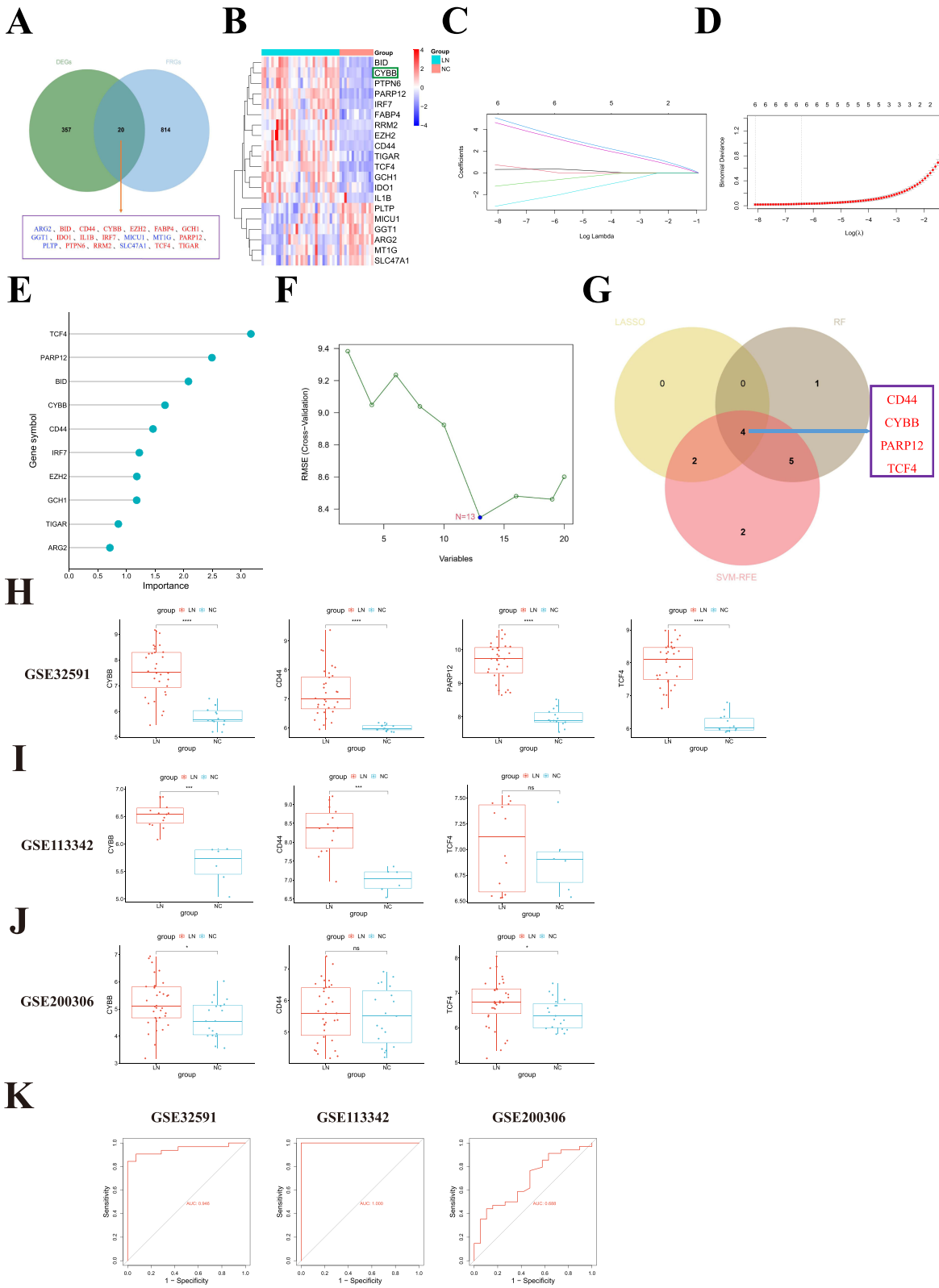

Figure 3 Acquisition of key FRGs in LN. (**A**) Venn plot of DEGs and FRGs. Red represents up-regulated DEGs and blue represents down-regulated DEGs. (**B**) Expression of DE-FRGs in LN and NC groups. The green box is the key ferroptosis-related genes of this study. (**C**) Path diagram of LASSO regression coefficients for DE-FRGs in the training set. (**D**) LASSO regression cross-validation curves. A 10-fold cross-validation was used in the training set to determine the optimal λ value. (**E**) The lollipop plot illustrates the relative importance of genes in the random forest model in the training set. (**F**) SVM-RFEs algorithm to screen feature genes. (**G**) Venn diagram shows candidate key genes. (**H**) Expression levels of candidate key genes in the training set. (**I–J**) Expression levels of candidate key genes in the validation sets. (**K**) ROC curves plotted based on CYBB gene expression profiles in the training and validation sets. Noted: * $P<0.05$, *** $P<0.001$, **** $P<0.0001$, ns $P>0.05$.

https://doi.org/10.2147/JIR.S527545

Table 3 The Results of Three Machine Learning Algorithms

Machine learning	Count	Gene symbol	Intersection Genes
LASSO	6	*CD44*, *CYBB*, *MICU1*, *PARP12*, *PLTP*, *TCF4*	*CD44*
RF	10	*TCF4*, *PARP12*, *BID*, *CD44*, *CYBB*, *IR7*, *EZH2*, *GCH1*, *TIGAR*, *ARG2*	*CYBB*
SVM-RFE	13	*TCF4*, *PARP12*, *CD44*, *EZH2*, *BID*, *PLTP*, *TIGAR*, *CYBB*, *MICU1*, *GCH1*, *ARG2*, *RRM2*, *IRF7*	*TCF4*
			PARP12

dendritic cells ($P < 0.05$), regulatory T cells ($P < 0.05$) and memory B cells into ($P < 0.05$) negative correlation (Figure 5C).

Clinical Sample Validation and Clinical Traits Correlation Analysis

In the NephroSeq V5 database, we observed that the expression level of *CYBB* was significantly higher in LN group than in NC group ($P < 0.0001$) (Figure 6A). Further correlation analysis of clinical traits revealed that *CYBB* was negatively

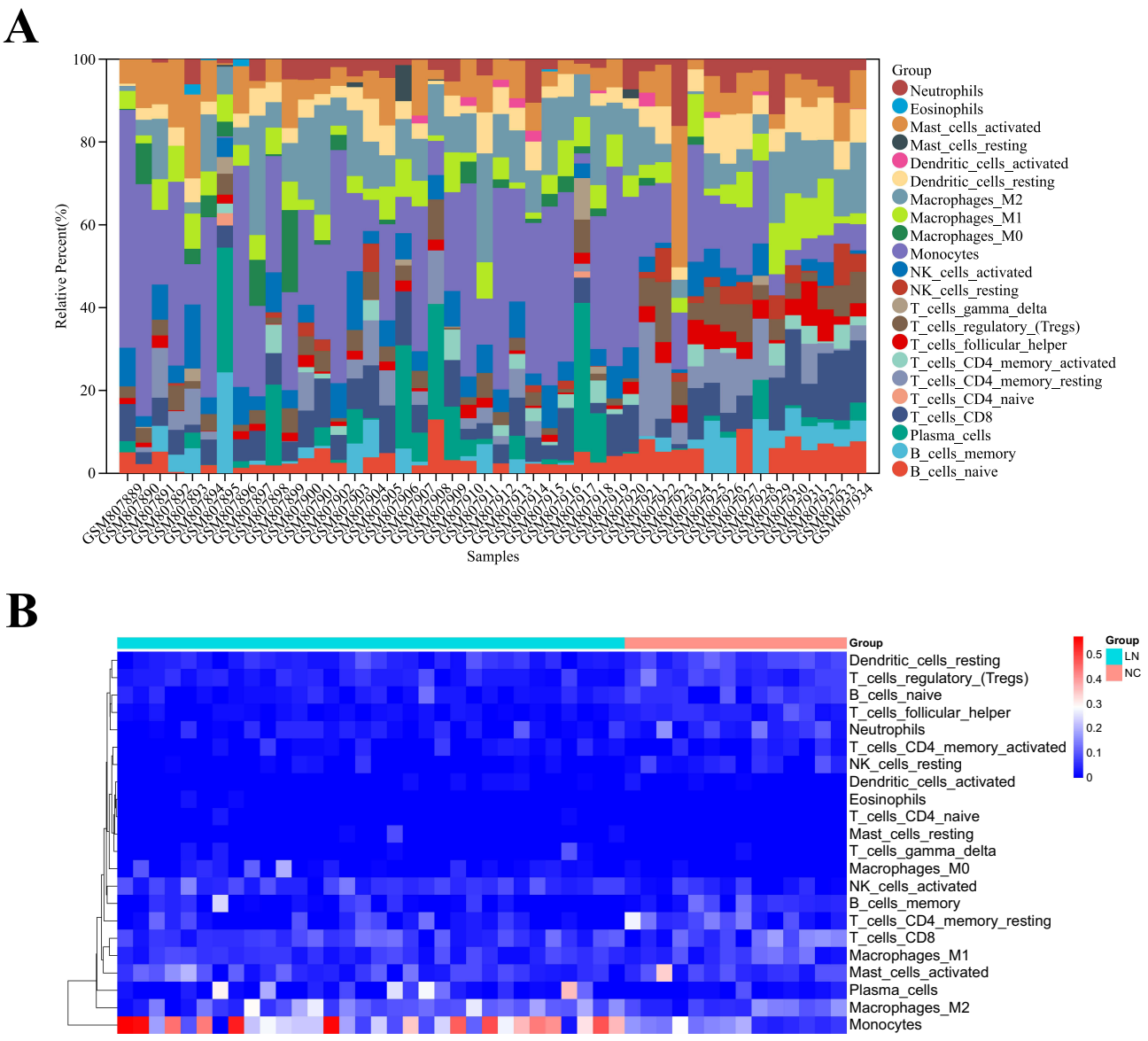

Figure 4 Analysis of immune cell infiltration in LN. (**A**) Relative percentage of immune cell subpopulations in 46 glomerular samples. (**B**) Heatmap of immune cell content in 46 samples.

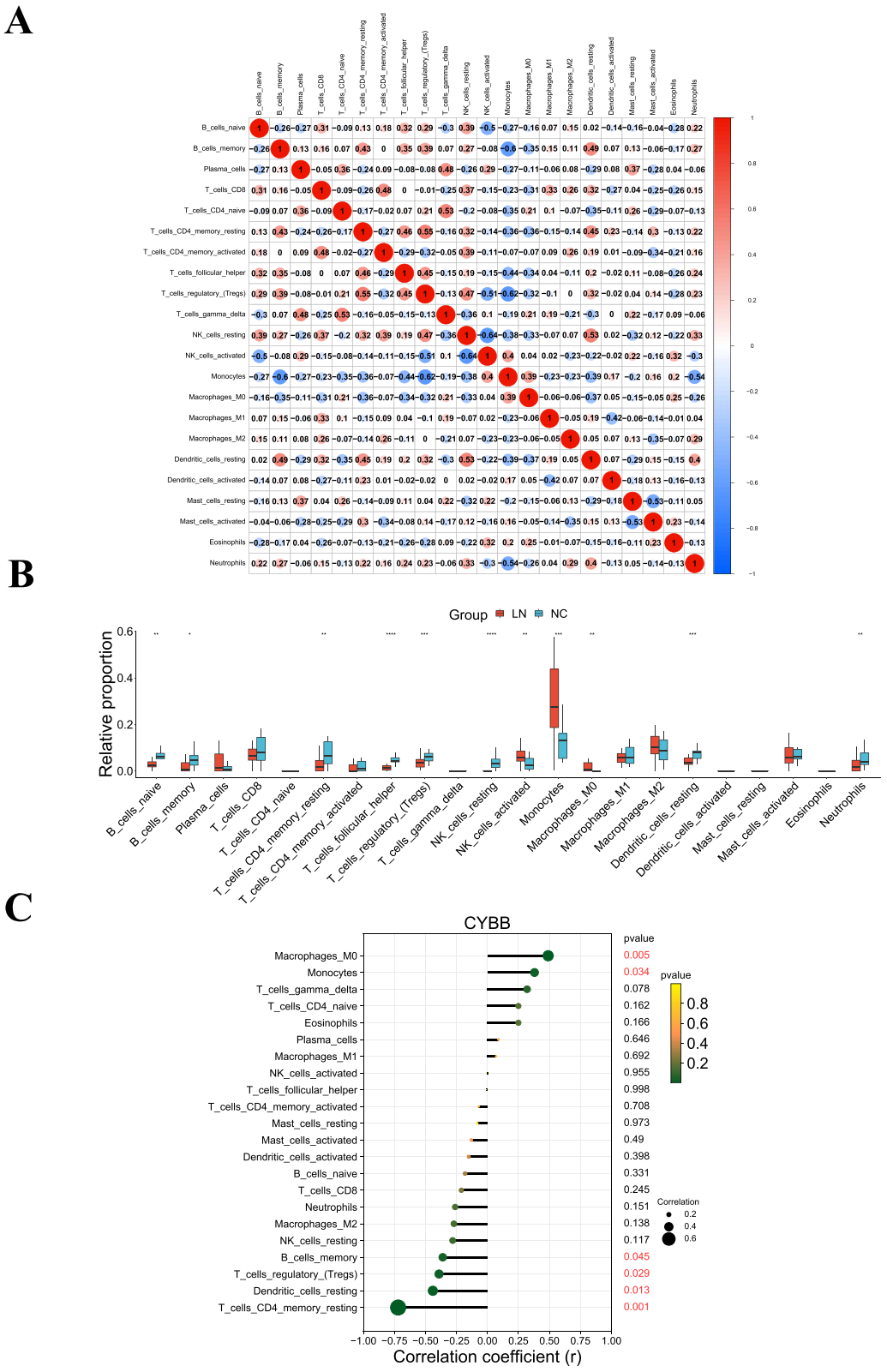

Figure 5 Analysis of immune cell infiltration in LN. (**A**) Correlation between immune cells in 22 in LN glomerular tissue. (**B**) Differential analysis of immune infiltrating cells between LN and NC. (**C**) Pearson correlation analysis of CYBB with immune infiltrating cells. Red text coloring represents *P*<0.05. Noted: * *P*<0.05, ** *P*<0.01, *** *P*<0.001, **** *P*<0.0001.

https://doi.org/10.2147/JIR.S527545

correlated with GFR ($R = -0.63$, $P = 0.00022$) (Figure 6B), and positively correlated with proteinuria ($R = 0.52$, $P = 0.0048$) and Scr levels ($R = 0.6$, $P = 0.00039$) (Figure 6C and D). It is further implied that *CYBB* may promote the development of LN. We found that the protein expression level of *ACSL4* (a key driver gene for ferroptosis)[49] was significantly higher in renal tissues of LN patients compared with NC group (Figure 6E and H). In contrast, the protein expression level of *GPX4* (a key protective gene for ferroptosis)[50] was significantly lower in the renal tissues of LN patients compared with the NC group (Figure 6F and H). As a result of our bioinformatics analysis, the expression level of *CYBB* in LN kidney tissues was significantly higher than that of the NC group (Figure 6G and H).

The Animal Experiments Verified the Overactivation of Ferroptosis in LN and the Expression of CYBB

We observed that 24h urine protein, splenic index, perinephric lymph node index and anti-dsDNA antibody were significantly higher in lpr group compared with control group (Figure 7A–D). Through PAS staining, diffuse proliferation of glomerular mesangial cells, infiltration of inflammatory cells, and formation of renal interstitial fibers in severe cases could be seen in lpr group (Figure 7E). IF stainings revealed massive deposition of glomerular C3 and IgG in the lpr

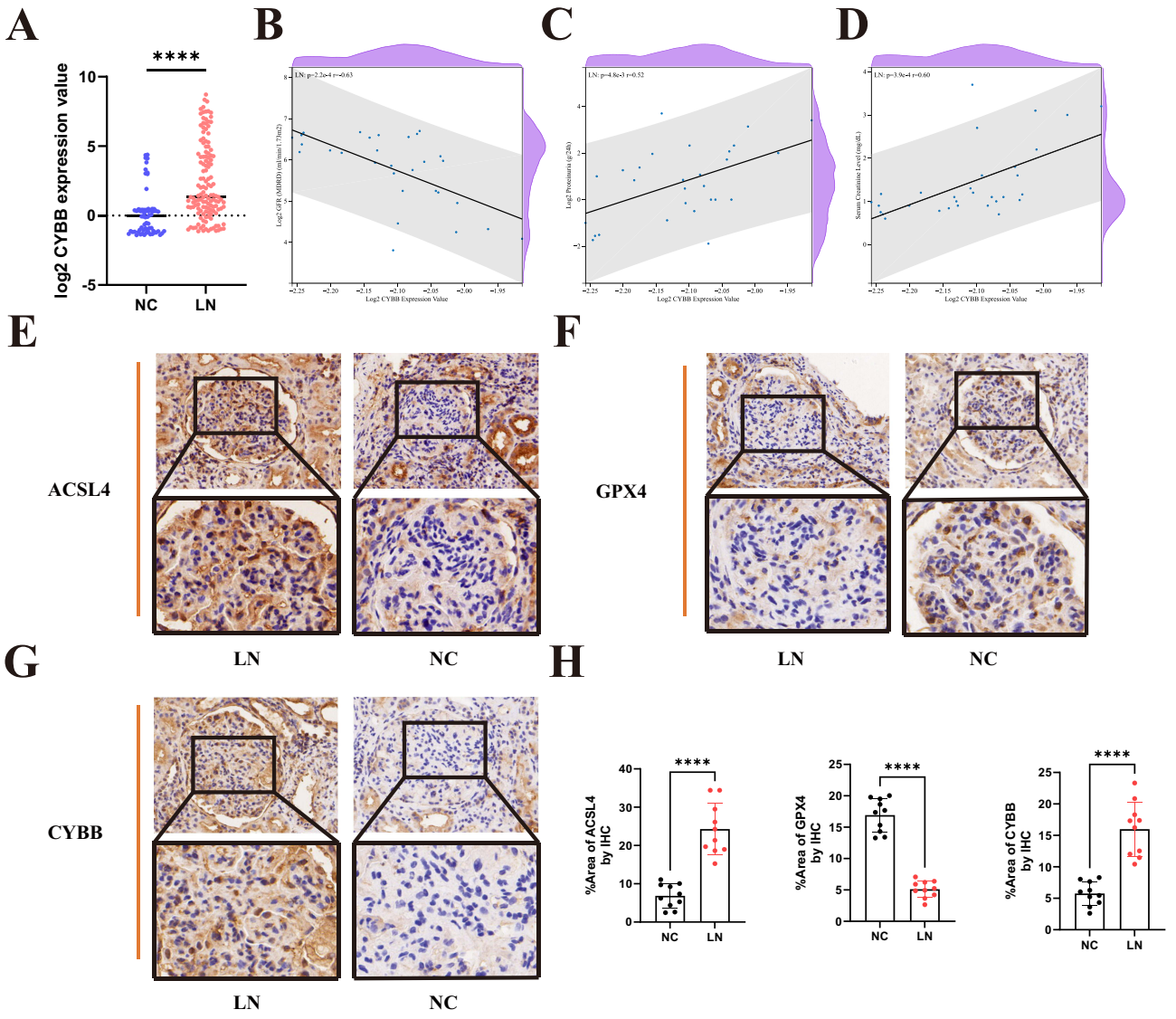

Figure 6 Clinical correlation analysis and clinical samples to validate the expression of *CYBB* and key genes for ferroptosis (*ACSL4* and *GPX4*). (**A**) Expression of CYBB in the Nephroseq database. (**B–D**) Correlation analysis of *CYBB* with GFR, proteinuria and Scr in LN. (**E–G**) IHC staining of ACSL4, GPX4 and CYBB in kidney sections. (**H**) The percentage of positive area in IHC staining. Noted: **** $P<0.0001$.

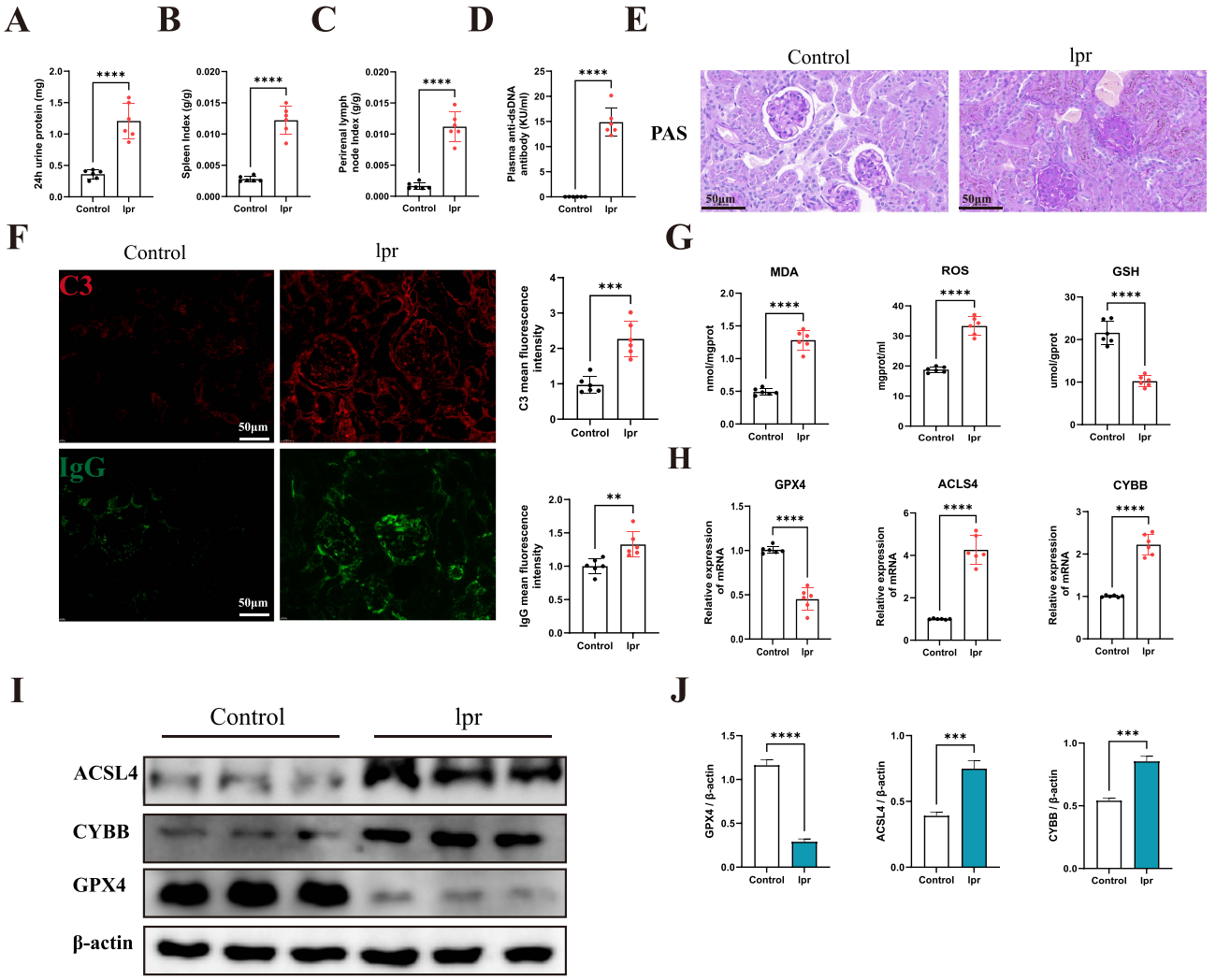

Figure 7 Animal experiments to validate the ferroptosis and *CYBB* expression. (**A–D**) The 24h urinary proteins, spleen index and perirenal lymph node index in mice of both groups. (**E**) The PAS staining in mice of both groups. (**F**) IF staining of C3 and IgG, and mean fluorescence intensity in both groups of mice. (**G**) The MDA, ROS and GSH in mice of both groups. (**H–J**) The mRNA and protein expression levels of *ACSL4*, *CYBB* and *GPX4* in both groups of mice. The grouping of blots from different gels, fields. Noted: ** *P*<0.01, *** *P*<0.001, **** *P*<0.0001.

group (Figure 7F). These favorably illustrate the successful construction of lupus mice model. MDA and ROS levels were significantly higher in the lpr group compared to those in the control group, whereas the opposite was true for GSH levels, implying that stronger lipid peroxidation occurred in lupus mice (Figure 7G). In order to validate our bioinformatics analysis results, we examined the expression levels of *ACSL4* and *GPX4* by Western blotting and RT-qPCR. We found that the expression levels of *ACSL4* and *CYBB* were significantly higher in lpr group than in control group, whereas the expression level of *GPX4* was significantly lower than in control group (Figure 7H–J). The above results revealed high CYBB expression and hyperactivation of ferroptosis in lupus mice.

Discussion

Ferroptosis is a form of programmed cell death that is dependent on iron ion catalysis and is triggered by the accumulation of lipid peroxides.[7] In recent years, iron death has been shown to play an important role in the development of a variety of diseases, including renal diseases and autoimmune diseases.[51] LN is one of the main manifestations of the severity of the disease in SLE. A growing body of research suggests that ferroptosis may be involved in the pathogenesis of LN, especially playing a key role in pro-inflammatory responses and cellular damage.[52] Therefore, in-depth exploration of ferroptosis-related genes and their regulatory mechanisms can help to reveal the pathological process of lupus nephritis and provide new targets for clinical

https://doi.org/10.2147/JIR.S527545

treatment. The results obtained in this study are highly consistent with the existing research data and further validate the important role of ferroptosis in lupus nephritis.

In this study, 377 DEGs of LN were screened at the transcriptome level. These DEGs were functionally annotated and analyzed for pathway enrichment, and PPI networks were constructed. Then four candidate key LNDE-FRGs, *CD44*, *CYBB*, *TCF4* and *PARP12*, were gained by three machine learning algorithms. The expression of *CYBB* was subsequently validated in two LN-related external datasets. The ROC analysis revealed that *CYBB* has a good diagnostic performance for LN. The NephronSeq V5 database also demonstrated a significant correlation between *CYBB* and clinical traits of LN. Subsequently, we explored the immune microenvironmental changes in LN kidneys. The correlation between *CYBB* and immune infiltration cells was analyzed. Eventually, clinical kidney tissue and animal experiments were further validated.

GO functional annotation displayed that these DEGs were mainly involved in the type I interferon signaling pathway and in the immune response involving neutrophil activation. Loss of tolerance to nucleic acids, blood interferons, and neutrophil characteristics are the three main features of SLE.[53] Free nucleic acids in LN patients are considered to be potent activators of type I interferons, and they can be recognized by intracellular nucleic acid sensors and activate the type I interferon signaling pathway thereby promoting the release of autoantibodies and inflammatory factors that exacerbate renal inflammation and injury.[54–56] Some studies have shown a progressive enrichment of neutrophil transcripts in SLE patients during progression to active LN, demonstrating that neutrophils play a key role in the immune dysregulation that triggers organ damage.[53] KEGG pathway analysis showed the most pronounced enrichment of DEGs phagosomes and natural killer cell-mediated cytotoxicity pathways. Myeloid phagocytes form phagosomes when stimulated by external microorganisms, resulting in the production of excessive inflammatory cytokines and the initiation of respiratory bursts to generate large amounts of ROS,[57] all of which may enhance renal inflammation and aggravate renal injury in LN. There is increasing evidence that NK cells also play a role in autoimmune diseases. NK cells have been found to aggregate in the glomerular region of LN and single-cell RNA sequencing of human LN renal tissues identified two populations of NK cells,[46,58] but the specific pathogenic role of NK cells in LN has not yet been reported.

The *CYBB* encodes the cytochrome b-245β chain, known as NADPH oxidase 2 (NOX2). In epithelial ovarian cancer, CYBB generates reactive oxygen species (ROS) by proton transfer, thereby contributing to the process of ferroptosis.[59] Previous studies have shown that inhibiting of ROS overproduction in lupus mice attenuates renal fibrosis.[21,60] Xu et al found CYBB upregulation and GPX4 downregulation in pre-eclamptic placental tissue. Meanwhile, knockdown of *CYBB* in trophoblast cells revealed reduced levels of ROS and lipid peroxidation, and restored GPX4 expression.[61] Variations in neutrophil cytoplasmic factor, an essential subunit of CYBB, promote auto-antibodies production and kidney injury in mice and SLE patients.[62] Therefore, whether CYBB is involved in LN pathogenesis by activating ferroptosis through the generation of ROS? It deserves further investigation, and no relevant reports have been seen yet. CYBB has also been previously reported to be one of the ferroptosis-related genes in LN, but it has not been verified by animal experiments.[63] The findings of the present study are consistent with the previous ones and its expression was verified in lupus mice, suggesting that regulation of CYBB expression may be a potential target for the treatment of LN.

Immune cell infiltration is a hallmark of LN. Researches have suggested that certain oxidative substances involved in iron metabolism can enhance the activation of inflammatory transcription factors induced by proteins and autoantibodies, leading to the production of cytokines, chemokines, and increased immune cell infiltration.[64] Abnormal immune cells such as $CD4^+$ T cells, macrophages, and dendritic cells play a role in the pathogenic mechanisms of systemic lupus erythematosus (SLE). These cells are recruited to kidney tissues where they release pro-inflammatory cytokines and chemokines, contributing to increased immune cell infiltration and tissue damage in patients with LN.[65] *CYBB* expression was found to be up-regulated in LN glomerular samples in this study and was positively correlated with M0 macrophages. This correlation implies that CYBB may contribute to LN progression by increasing macrophage infiltration through ferroptosis. Studies on SLE have revealed that plasmacytoid dendritic cells (pDCs) activated by oxidized mitochondrial DNA induce the generation of a subset of $CD4^+$ memory T cells. These T cells have a unique metabolic profile promotes ROS accumulation and of succinate secretion.[66] However, in our study, the expression of $CD4^+$ memory T cells in LN glomerular samples was lower than that in healthy controls. Hence, the specific relationship between *CYBB*, $CD4^+$ memory T cells, and LN need further investigation. Furthermore, the inability of dendritic cells to effectively clear dead cells has been suggested a pathogenic mechanism in LN. Self-antigens carried by cells that are not cleared are part of the immune complexes deposited in the kidneys.[67] *CYBB* was negatively correlated with resting dendritic cells, suggesting that the ability to clear self-antigens might be reduced and thus involved in the pathogenesis of LN. This suggest that *CYBB* is a reliable biomarker of LN.

GPX4 specifically scavenges lipid peroxides and is an important negative regulator of ferroptosis.[50] ACSL4 is a key enzyme in the lipid peroxidation process, which is critical for the onset of ferroptosis.[49] To explore whether ferroptosis occurs in lupus mice, we tested both of these factors in lupus mice. As in our analysis, GPX4 expression levels were reduced, while ACSL4 and CYBB expression levels were increased. In addition, we detected elevated levels of the lipid peroxide indicators MDA and ROS in lupus mice. This strongly suggests that CYBB may be involved in the pathogenesis of LN by promoting the occurrence of ferroptosis.

Of course, our study has limitations. Firstly, our data were sourced from the GEO public database, which involves secondary mining and analysis of previously published data. This could have introduced bias into the results. Secondly, the number of samples included in our study was relatively small, which may have increased the likelihood of false positives. Lastly, our results are based on bioinformatic methods. Therefore, further experiments are required to explore the expression levels of CYBB mediated pathway proteins and the effects of regulating CYBB expression on ferroptosis.

Conclusion

In summary, *CYBB* expression was elevated in LN. In addition, *CYBB* was associated with immune cell infiltration in LN, suggesting its role in the immune microenvironment. In general, our study implied that *CYBB* may be a good ferroptosis-related biomarker for LN.

Author Information

Su Zhang is now affiliated with the “Department of Rheumatology, The Nanping First Affiliated Hospital of Fujian Medical University, Nanping, People’s Republic of China.

Data Sharing Statement

The datasets generated and/or analysed during the current study are available in the [GEO] repository, [https://www.ncbi.nlm.nih.gov/geo/query/acc.cgi?acc=GSE32591].

Acknowledgments

We thank all those who participated in this study.

Author Contributions

All authors made a significant contribution to the work reported, whether that is in the conception, study design, execution, acquisition of data, analysis and interpretation, or in all these areas; took part in drafting, revising or critically reviewing the article; gave final approval of the version to be published; have agreed on the journal to which the article has been submitted; and agree to be accountable for all aspects of the work.

Funding

This work was supported by the Joint funds for the innovation of science and technology, Fujian province (Grant number: 2023Y9236) and the Natural Science Foundation of Fujian Province (Grant number: 2024J01686).

Disclosure

The authors declare no competing interests.

References

1. Almaani S, Meara A, Rovin BH. Update on lupus nephritis. *Clin J Am Soc Nephrol*. 2017;12(5):825–835. doi:10.2215/CJN.05780616
2. Bingham KS, DiazMartinez J, Green R, et al. Longitudinal relationships between cognitive domains and depression and anxiety symptoms in systemic lupus erythematosus. *Semin Arthritis Rheumatism*. 2021;51(6):1186–1192. doi:10.1016/j.semarthrit.2021.09.008
3. Kant S, Kronbichler A, Sharma P, Geetha D. Advances in understanding of pathogenesis and treatment of immune-mediated kidney disease: a review. *Am J Kidney Dis*. 2022;79(4):582–600. doi:10.1053/j.ajkd.2021.07.019
4. Mejia-Vilet JM, Malvar A, Arazi A, Rovin BH. The lupus nephritis management renaissance. *Kidney Int*. 2022;101(2):242–255. doi:10.1016/j.kint.2021.09.012
5. Kostopoulou M, Pitsigavdaki S, Bertsias G. Lupus nephritis: improving treatment options. *Drugs*. 2022;82(7):735–748. doi:10.1007/s40265-022-01715-1

6. O'Shea K, Misra BB. Software tools, databases and resources in metabolomics: updates from 2018 to 2019. *Metabolomics*. 2020;16(3):36. doi:10.1007/s11306-020-01657-3
7. Dixon SJ, Lemberg KM, Lamprecht MR, et al. Ferroptosis: an iron-dependent form of nonapoptotic cell death. *Cell*. 2012;149(5):1060–1072. doi:10.1016/j.cell.2012.03.042
8. Stockwell BR, Friedmann Angeli JP, Bayir H, et al. Ferroptosis: a regulated cell death nexus linking metabolism, redox biology, and disease. *Cell*. 2017;171(2):273–285. doi:10.1016/j.cell.2017.09.021
9. Gao M, Monian P, Quadri N, Ramasamy R, Jiang X. Glutaminolysis and transferrin regulate ferroptosis. *Molecular Cell*. 2015;59(2):298–308. doi:10.1016/j.molcel.2015.06.011
10. Del Re DP, Amgalan D, Linkermann A, Liu Q, Kitsis RN. Fundamental mechanisms of regulated cell death and implications for heart disease. *Physiol Rev*. 2019;99(4):1765–1817. doi:10.1152/physrev.00022.2018
11. Li Y, Feng D, Wang Z, et al. Ischemia-induced ACSL4 activation contributes to ferroptosis-mediated tissue injury in intestinal ischemia/reperfusion. *Cell Death Differ*. 2019;26(11):2284–2299. doi:10.1038/s41418-019-0299-4
12. Mayr L, Grabherr F, Schwärzler J, et al. Dietary lipids fuel GPX4-restricted enteritis resembling Crohn's disease. *Nat Commun*. 2020;11(1):1775. doi:10.1038/s41467-020-15646-6
13. Wang Y, Zhang M, Bi R, et al. ACSL4 deficiency confers protection against ferroptosis-mediated acute kidney injury. *Redox Biol*. 2022;51:102262. doi:10.1016/j.redox.2022.102262
14. Lu Y, Qin H, Jiang B, et al. KLF2 inhibits cancer cell migration and invasion by regulating ferroptosis through GPX4 in clear cell renal cell carcinoma. *Cancer Lett*. 2021;522:1–13. doi:10.1016/j.canlet.2021.09.014
15. Zhang X, Li LX, Ding H, Torres VE, Yu C, Li X. Ferroptosis promotes cyst growth in autosomal dominant polycystic kidney disease mouse models. *J Am Soc Nephrol*. 2021;32(11):2759–2776. doi:10.1681/ASN.2021040460
16. Niki E. Biomarkers of lipid peroxidation in clinical material. *BBA*. 2014;1840(2):809–817. doi:10.1016/j.bbagen.2013.03.020
17. Ames PR, Alves J, Murat I, Isenberg DA, Nourooz-Zadeh J. Oxidative stress in systemic lupus erythematosus and allied conditions with vascular involvement. *Rheumatology*. 1999;38(6):529–534. doi:10.1093/rheumatology/38.6.529
18. Mansour RB, Lassoued S, Gargouri B, Gaïd A E, Attia H, Fakhfakh F. Increased levels of autoantibodies against catalase and superoxide dismutase associated with oxidative stress in patients with rheumatoid arthritis and systemic lupus erythematosus. *Scand J Rheumatol*. 2008;37(2):103–108. doi:10.1080/03009740701772465
19. Marks ES, Bonnemaison ML, Brusnahan SK, et al. Renal iron accumulation occurs in lupus nephritis and iron chelation delays the onset of albuminuria. *Sci Rep*. 2017;7(1):12821. doi:10.1038/s41598-017-13029-4
20. Monteith AJ, Kang S, Scott E, et al. Defects in lysosomal maturation facilitate the activation of innate sensors in systemic lupus erythematosus. *Proc Natl Acad Sci USA*. 2016;113(15):E2142–2151. doi:10.1073/pnas.1513943113
21. Sule G, Abuaita BH, Steffes PA, et al. Endoplasmic reticulum stress sensor IRE1α propels neutrophil hyperactivity in lupus. *J Clin Invest*. 2021;131(7). doi:10.1172/JCI137866
22. Scindia Y, Wlazlo E, Ghias E, et al. Modulation of iron homeostasis with hepcidin ameliorates spontaneous murine lupus nephritis. *Kidney Int*. 2020;98(1):100–115. doi:10.1016/j.kint.2020.01.025
23. van Raaij S, van Swelm R, Bouman K, et al. Tubular iron deposition and iron handling proteins in human healthy kidney and chronic kidney disease. *Sci Rep*. 2018;8(1):9353. doi:10.1038/s41598-018-27107-8
24. Hassan SZ, Gheita TA, Kenawy SA, Fahim AT, El-Sorougy IM, Abdou MS. Oxidative stress in systemic lupus erythematosus and rheumatoid arthritis patients: relationship to disease manifestations and activity. *Int J Rheum Dis*. 2011;14(4):325–331. doi:10.1111/j.1756-185X.2011.01630.x
25. Li P, Jiang M, Li K, et al. Glutathione peroxidase 4-regulated neutrophil ferroptosis induces systemic autoimmunity. *Nat Immunol*. 2021;22(9):1107–1117. doi:10.1038/s41590-021-00993-3
26. Theut LR, Dsouza DL, Grove RC, Boesen EI. Evidence of renal iron accumulation in a male mouse model of lupus. *Front Med*. 2020;7(516). doi:10.3389/fmed.2020.00516
27. Oh VM. Iron dextran and systemic lupus erythematosus. *BMJ*. 1992;305(6860):1000. doi:10.1136/bmj.305.6860.1000-a
28. Brown AC. Lupus erythematosus and nutrition: a review of the literature. *J Ren Nutr*. 2000;10(4):170–183. doi:10.1053/jren.2000.16323
29. Edgar R, Domrachev M, Lash AE. Gene expression omnibus: NCBI gene expression and hybridization array data repository. *Nucleic Acids Res*. 2002;30(1):207–210. doi:10.1093/nar/30.1.207
30. Berthier CC, Bethunaickan R, Gonzalez-Rivera T, et al. Cross-species transcriptional network analysis defines shared inflammatory responses in murine and human lupus nephritis. *J Immunol*. 2012;189(2):988–1001. doi:10.4049/jimmunol.1103031
31. Mejia-Vilet JM, Parikh SV, Song H, et al. Immune gene expression in kidney biopsies of lupus nephritis patients at diagnosis and at renal flare. *Nephrol Dial Transplant*. 2019;34(7):1197–1206. doi:10.1093/ndt/gfy125
32. Parikh SV, Malvar A, Song H, et al. Molecular profiling of kidney compartments from serial biopsies differentiate treatment responders from non-responders in lupus nephritis. *Kidney Int*. 2022;102(4):845–865. doi:10.1016/j.kint.2022.05.033
33. Ritchie ME, Phipson B, Wu D, et al. limma powers differential expression analyses for RNA-sequencing and microarray studies. *Nucleic Acids Res*. 2015;43(7):e47. doi:10.1093/nar/gkv007
34. Xu S, Hu E, Cai Y, et al. Using clusterProfiler to characterize multiomics data. *Nature Protocols*. 2024;19(11):3292–3320. doi:10.1038/s41596-024-01020-z
35. Franceschini A, Szklarczyk D, Frankild S, et al. STRING v9.1: protein-protein interaction networks, with increased coverage and integration. *Nucleic Acids Res*. 2013;41(Database issue):D808–815. doi:10.1093/nar/gks1094
36. Doncheva NT, Morris JH, Holze H, et al. Cytoscape stringApp 2.0: analysis and visualization of heterogeneous biological networks. *J Proteome Res*. 2023;22(2):637–646. doi:10.1021/acs.jproteome.2c00651
37. Bandettini WP, Kellman P, Mancini C, et al. MultiContrast Delayed Enhancement (MCODE) improves detection of subendocardial myocardial infarction by late gadolinium enhancement cardiovascular magnetic resonance: a clinical validation study. *J Cardiovasc Magn Reson*. 2012;14(1):83. doi:10.1186/1532-429X-14-83
38. Zhou N, Yuan X, Du Q, et al. FerrDb V2: update of the manually curated database of ferroptosis regulators and ferroptosis-disease associations. *Nucleic Acids Res*. 2023;51(D1):D571–d582. doi:10.1093/nar/gkac935
39. Cheung-Lee WL, Link AJ. Genome mining for lasso peptides: past, present, and future. *J Indus Microbiol Biotechnol*. 2019;46(9–10):1371–1379. doi:10.1007/s10295-019-02197-z

40. Friedman J, Hastie T, Tibshirani R. Regularization paths for generalized linear models via coordinate descent. *J Stat Softw*. 2010;33(1):1–22. doi:10.18637/jss.v033.i01
41. Rigatti SJ. Random Forest. *J Insur Med*. 2017;47(1):31–39. doi:10.17849/insm-47-01-31-39.1
42. Sanz H, Valim C, Vegas E, Oller JM, Reverter F. SVM-RFE: selection and visualization of the most relevant features through non-linear kernels. *BMC Bioinf*. 2018;19(1):432. doi:10.1186/s12859-018-2451-4
43. Robin X, Turck N, Hainard A, et al. pROC: an open-source package for R and S+ to analyze and compare ROC curves. *BMC Bioinf*. 2011;12(77). doi:10.1186/1471-2105-12-77
44. Eddy S, Mariani LH, Kretzler M. Integrated multi-omics approaches to improve classification of chronic kidney disease. *Nat Rev Nephrol*. 2020;16(11):657–668. doi:10.1038/s41581-020-0286-5
45. Newman AM, Liu CL, Green MR, et al. Robust enumeration of cell subsets from tissue expression profiles. *Nature Methods*. 2015;12(5):453–457. doi:10.1038/nmeth.3337
46. Arazi A, Rao DA, Berthier CC, et al. The immune cell landscape in kidneys of patients with lupus nephritis. *Nat Immunol*. 2019;20(7):902–914. doi:10.1038/s41590-019-0398-x
47. Kwant LE, Vegting Y, Tsang ASMWP, et al. Macrophages in lupus nephritis: exploring a potential new therapeutic avenue. *Autoimmunity Rev*. 2022;21(12):103211. doi:10.1016/j.autrev.2022.103211
48. Richoz N, Tuong ZK, Loudon KW, et al. Distinct pathogenic roles for resident and monocyte-derived macrophages in lupus nephritis. *JCI Insight*. 2022;7(21). doi:10.1172/jci.insight.159751
49. Liu L, Kang XX. ACSL4 is overexpressed in psoriasis and enhances inflammatory responses by activating ferroptosis. *Biochem Biophys Res Commun*. 2022;623:1–8. doi:10.1016/j.bbrc.2022.07.041
50. Gao M, Yi J, Zhu J, et al. Role of mitochondria in ferroptosis. *Molecular Cell*. 2019;73(2):354–363.e353. doi:10.1016/j.molcel.2018.10.042
51. Shen L, Wang X, Zhai C, Chen Y. Ferroptosis: a potential therapeutic target in autoimmune disease (Review). *Exp Ther Med*. 2023;26(2):368. doi:10.3892/etm.2023.12067
52. Chen X, Kang R, Kroemer G, Tang D. Ferroptosis in infection, inflammation, and immunity. *J Exp Med*. 2021;218(6). doi:10.1084/jem.20210518
53. Banchereau R, Hong S, Cantarel B, et al. Personalized immunomonitoring uncovers molecular networks that stratify lupus patients. *Cell*. 2016;165(3):551–565. doi:10.1016/j.cell.2016.03.008
54. Unterholzner L, Keating SE, Baran M, et al. IFI16 is an innate immune sensor for intracellular DNA. *Nat Immunol*. 2010;11(11):997–1004. doi:10.1038/ni.1932
55. Pham PT, Bavuu O, Kim-Kaneyama JR, et al. Innate immune system regulated by stimulator of interferon genes, a cytosolic DNA sensor, regulates endothelial function. *J Am Heart Assoc*. 2023;12(22):e030084. doi:10.1161/JAHA.123.030084
56. Takaoka A, Wang Z, Choi MK, et al. DAI (DLM-1/ZBP1) is a cytosolic DNA sensor and an activator of innate immune response. *Nature*. 2007;448(7152):501–505. doi:10.1038/nature06013
57. Fitzgerald KA, Kagan JC. Toll-like receptors and the control of immunity. *Cell*. 2020;180(6):1044–1066. doi:10.1016/j.cell.2020.02.041
58. Scheffschick A, Fuchs S, Malmström V, Gunnarsson I, Brauner H. Kidney infiltrating NK cells and NK-like T-cells in lupus nephritis: presence, localization, and the effect of immunosuppressive treatment. *Clin Exp Immunol*. 2022;207(2):199–204. doi:10.1093/cei/uxab035
59. Yang WH, Huang Z, Wu J, Ding CC, Murphy SK, Chi JT. A TAZ-ANGPTL4-NOX2 axis regulates ferroptotic cell death and chemoresistance in epithelial ovarian cancer. *Mol Cancer Res*. 2020;18(1):79–90. doi:10.1158/1541-7786.MCR-19-0691
60. Tian J, Huang T, Chen J, et al. SIRT1 slows the progression of lupus nephritis by regulating the NLRP3 inflammasome through ROS/TRPM2/Ca(2+) channel. *Clin Exp Med*. 2023;23(7):3465–3478. doi:10.1007/s10238-023-01093-2
61. Xu X, Zhu M, Zu Y, Wang G, Li X, Yan J. Nox2 inhibition reduces trophoblast ferroptosis in preeclampsia via the STAT3/GPX4 pathway. *Life Sci*. 2024;343(122555):122555. doi:10.1016/j.lfs.2024.122555
62. Geng L, Zhao J, Deng Y, et al. Human SLE variant NCF1-R90H promotes kidney damage and murine lupus through enhanced Tfh2 responses induced by defective efferocytosis of macrophages. *Ann Rheumatic Dis*. 2022;81(2):255–267. doi:10.1136/annrheumdis-2021-220793
63. Wang W, Lin Z, Feng J, et al. Identification of ferroptosis-related molecular markers in glomeruli and tubulointerstitium of lupus nephritis. *Lupus*. 2022;31(8):985–997. doi:10.1177/09612033221102076
64. Wlazlo E, Mehrad B, Morel L, Scindia Y. Iron metabolism: an under investigated driver of renal pathology in lupus nephritis. *Front Med*. 2021;8(643686). doi:10.3389/fmed.2021.643686
65. Khan SQ, Khan I, Gupta V. CD11b activity modulates pathogenesis of lupus nephritis. *Front Med*. 2018;5(52). doi:10.3389/fmed.2018.00052
66. Allison SJ. A CD4(+) T cell population provides B cell help in SLE. *Nat Rev Rheumatol*. 2019;15(2):63. doi:10.1038/s41584-018-0150-1
67. Tsai F, Perlman H, Cuda CM. The contribution of the programmed cell death machinery in innate immune cells to lupus nephritis. *Clin Immunol*. 2017;185:74–85. doi:10.1016/j.clim.2016.10.007